

Supporting Information

Structural and Thermal Photobehaviour Characterizations of $(DPA)_2MnBr_4$: An Environmentally Friendly Organic-Inorganic Hybrid Metal Halide Perovskite with a Reversible Emission Colour Switching for Anti-Counterfeiting and Solvent Vapours Photosensing

Asmae Ben Abdelhadi,^{a,b}[§] Francisco Sánchez,^{a,§} Mario Gutiérrez,^a Boiko Cohen,^a Luis Lezama^c and Abderrazzak Douhal^{a,*}

^a Departamento de Química Física, Facultad de Ciencias Ambientales y Bioquímica, e INAMOL, Campus Tecnológico de Toledo, Universidad de Castilla-La Mancha (UCLM), Avenida Carlos III, S.N., 45071 Toledo, Spain.

^b Engineering Laboratory of Organometallic, Molecular Materials, and Environment (LIMOME), Faculty of Sciences, Sidi Mohamed Ben Abdellah University, 30000, Fez, Morocco.

^c Departamento de Química Orgánica e Inorgánica, Facultad de Ciencia y Tecnología, Universidad del País Vasco, UPV/EHU, B Sarriena s/n, 48940 Leioa, Spain.

[§]equal contributions.

*Corresponding author: Abderrazzak.Douhal@uclm.es (A. D.)

Index

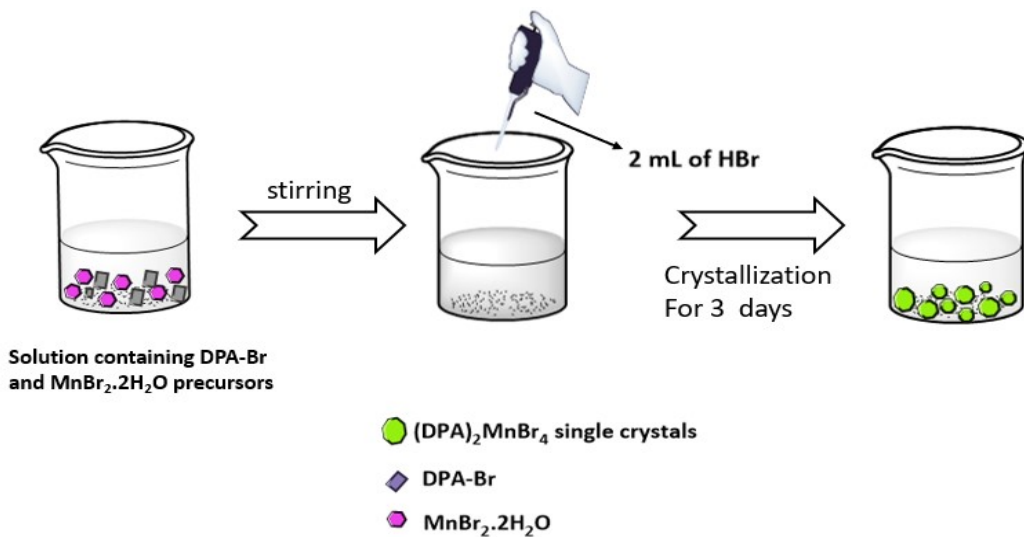
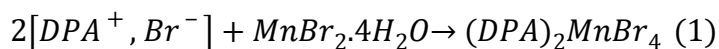
Section 1 – Experimental Section	Page 4
Section 1.1 – Chemical reagents	Page 4
Section 1.2 – Growth of 1 single crystal	Page 4
Section 1.3 – Formation of 1 powder	Page 4
Section 1.4 – Fabrication of green light-emitting diodes (LEDs)	. Page 5
Section 1.5 – Preparation of 1 strips	Page 5
Section 1.6 – Characterizations and measurements	Pages 6-8
Figure S1. A) X-band and Q-band. B) electron-spin paramagnetic resonance (EPR) of 1 at RT	
	Page 8
Figure S2. Thermal evolution of the X-band EPR spectrum of 1 from 295 to 423 K.	Page 8
Figure S3. X-band EPR spectra recorded before and after the sample was heated to 433 K and left at room temperature for the time indicated.	Page 9
Figure S4. A) Excitation spectra of 1 collected at different emission wavelengths of (300–580 nm). B) Excitation wavelength-dependent (365–450 nm) emission spectra of 1 .	Page 10
Figure S5. A) Correlation between the shortest Mn-Mn distances and photoluminescence quantum yield (PLQY), B) and C) Correlation between closest Mn-Mn distances and the non-radiative rate constant K_{nr} in Mn-Based tetrahedral hybrid perovskites.	Page 10
Figure S6. Change in the emission intensity maximum with days of 1 .	Page 11
Figure S7. Excitation spectra of 1 at different temperature. The observation wavelength is 650 nm.	Page 11
Figure S8. Recover in the emission intensity maximum (at 540 nm) during the cooling process of 1 .	Page 12

Table S1. Crystal data and structure refinement for 1 at 296K.	Page 13
Table S2. Fractional atomic coordinates and isotropic or equivalent isotropic displacement parameters (\AA^2) for 1 .	Page 13
Table S3. Atomic displacement parameters (\AA^2) for 1 .	Page 15
Table S4. Geometric parameters (\AA , $\text{\textcircled{d}}$) for 1 .	Page 15
Table S5. Hydrogen-bond geometry (\AA , $\text{\textcircled{d}}$) for 1 .	Page 16
Tables S6. Comparison of the emission parameters of Mn-based tetrahedral hybrid perovskites, including: the shortest Mn-Mn distances, emission wavelength (λ_{em}), PLQY lifetime and Knr.	Page 16
References	Page 19
Acknowledgment	Page 20
Conflicts of interest	Page 21

Experimental section

Chemical reagent. All chemicals were of reagent grade and were used without further purification. The materials are di-n-propylammonium bromide (99% aq. soln.), purchased from Sigma Aldrich (Madrid, Spain), manganese (II) bromide tetrahydrate ($MnBr_2 \cdot 4H_2O$, 98%) obtained from Acros Organics (Madrid, Spain), Hydrobromic acid (HBr, 48% w/w aq. soln.) and Anhydrous methanol (99.7%) obtained from Alfa Aesar (Madrid, Spain).

Growth of 1 single Crystals. The single crystals of **1** were synthesized by a simple solution-phase crystallization method. In a typical experiment, 0.364 g (2 mmol) of di-n-propylammonium bromide (DPA-Br) and 0.286 g (1 mmol) of manganese (II) bromide tetrahydrate ($MnBr_2 \cdot 4H_2O$) were added to an aqueous solution which contains 2 mL of 80% HBr under stirring for 2h at room temperature to allow the raw materials to react completely. Light green crystals were obtained when the solution was evaporated to almost dryness at 318 K in an oven after 4 days. Finally, the crystals were washed with ethyl acetate and dried in a vacuum overnight. The corresponding chemical reaction is given by equation 1 and the detailed procedure for the growth of **1** single crystals is shown in **Scheme S1**:



Scheme S1. Schematic illustration of the basic steps for the growth of the single crystals of **1**.

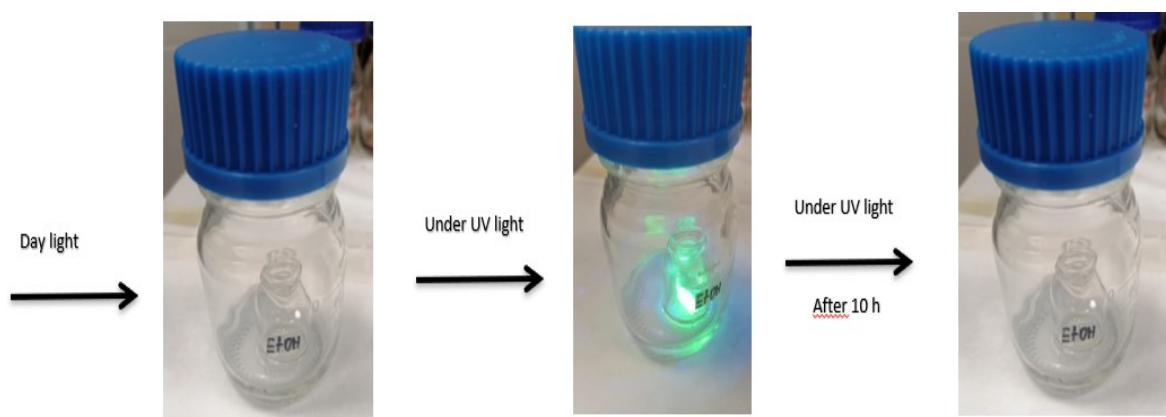
Synthesis of 1 powder. 0.182 g (1 mmol) of DPA-Br and 0.286 g (1 mmol) of $MnBr_2 \cdot 4H_2O$ were mixed in 4 mL of anhydrous methanol solvent for 2h at room temperature. Later, the solution

was kept at 313K for several days until the solvent was completely evaporated and a light-yellow powder of **1** was obtained.

The as-synthesized products showed a bright green fluorescence under UV light irradiation and were kept in a desiccator to prevent moisture exposure.

Fabrication of greenish-light-emitting diode LEDs. The down-converter LED devices were fabricated by depositing an amount of 10 mg of the as-synthesized **1** powder onto a blue chip (465 nm, 10 W, 9–11 V), which was used as the excitation light source to maximize the compound's luminescence. The down-converted LEDs were operated at 2.7 V at two different applied voltages of 2.6 V (5 mA) and 2.7 V (20 mA).

Preparation of **1 strip.** The typical experiment for the preparation of the stripes used in the vapochromism experiment is as follows: First, **1** perovskite was dissolved in MeOH with gentle heat until the formation of a concentrated solution which exhibited a red emission under UV light irradiation, then we added one drop of this concentrated solution per strip and heated (the temperature of the hot plate should be less than 353K), which caused the direct precipitation of the perovskite powder on the filter paper. Finally, the dried stripes show green emission at room temperature under UV light. Next, the paper stripe was placed in a small bottle and this small bottle was exposed to a saturated atmosphere of the solvent vapor for 30 to 50 min as is shown in **Scheme S2**. It should be noted that when the interaction occurs the paper stripe loses its green color under UV light.



Scheme S2. An example of the vapochromic experiment using a saturated atmosphere of the ethanol solvent vapor.

Characterizations and measurements

For the single crystal's experiments, a suitable crystal of **1** with dimensions $0.09 \times 0.06 \times 0.05$ mm³ was selected and placed on a MiTeGen micromount on a XtaLAB Synergy R, HyPix-Arc 100 diffractometer. The crystal was kept at 296.00(14) K during data collection using graphite monochromatic MoK α radiation ($\lambda = 0.71073\text{\AA}$). Using Olex2 , the structure was solved with the olex2.solve¹ structure solution program using Charge Flipping and refined with the SHELXL² refinement package using Least Squares minimization. Hydrogen atom positions were calculated geometrically and refined using the riding model. Important structural refinement parameters are summarized in Table S1-3 and the crystallographic data are also supplied. The MERCURY program was used for the crystal structure plotting. The crystallographic data are deposited in the Cambridge Crystallographic Data Centre (CCDC code 2434792). The data can be downloaded from the site (www.ccdc.cam.ac.uk/data_request/cif).

Hirshfeld surfaces analysis. the Hirshfeld surfaces mapped with d_{norm} and 2D fingerprint plots of **1** were generated using the Crystal-Explorer 3.1, enables identification of the regions of particular importance to intermolecular interactions; The normalized contact distance (d_{norm}) is based on both d_e and d_i (where d_e is the distance from the surface to the nearest atom exterior to the surface and d_i is the distance from the surface to the nearest atom interior to the surface) and r^{vdw} the van der Waals radii of the atom, as given by Equation2:

$$d_{norm} = \frac{(d_i - r_i^{vdw})}{r_i^{vdw}} + \frac{(d_e - r_e^{vdw})}{r_e^{vdw}} \quad (2)$$

The graphical plots of the molecular Hirshfeld surfaces mapped with d_{norm} used a red-white-blue color scheme, in which the red highlights shorter contacts, white represents the contact around VdW separation, and blue is for longer contact in order to identify the regions of particular importance to the intermolecular interactions. In addition, other graphical plots representing shape index and curvedness based on local curvatures are also presented.

Powder X-ray diffraction (PXRD). PXRD of the as-prepared powder **1** was carried out using a PANalytical diffractometer (X'Pert Pro model) and an X Bruker D8 Advance using a CuK α radiation (1.5418\AA) with a 2θ range of 5-50°. The conditions used were 45 kV, 40 mA and a

system of slits (soller-mask-divergence-antscatter) of 0.04 rad-10 mm-1/8° -1/4° with an X'celerator detector.

Thermogravimetric analysis (TGA) and differential scanning calorimetry (DSC) analysis. TGA-DSC analysis for the investigated compound **1** was performed in the temperature range of 30 to 890°C using the « SDT Q600 calorimeter ». The sample weight was 3 mg. The heating speed rate was 278 K/min using a platinum crucible under nitrogen flow (100 mL/min).

Electron-spin paramagnetic resonance (EPR). X-band (\sim 9.36 GHz) EPR measurements were carried out on a Bruker ELEXSYS 500 spectrometer equipped with a super-high-Q resonator ER-4123-SHQ and standard Oxford Instruments low-temperature devices. Q-band (\sim 33.9 GHz) EPR spectra were recorded on a Bruker EMX system equipped with an ER-510-QT resonator. The magnetic field was calibrated by a NMR probe and the frequency inside the cavity was determined with a Hewlett-Packard 5352B microwave frequency counter. Data were collected and processed using the Bruker Xepr suite.

The UV/Vis diffuse reflectance (DR) spectra were recorded on a JASCO V-670 spectrophotometer equipped with a 60 mm integrating sphere unit (JASCOISN-723). The longitudinal axes of the spectrum were converted using the Kubelka–Munk function from reflectance (%R) to K-M unit $F(R) = ((1 - R)^2(2R) - 1)$ where R is the diffuse reflectance intensity from the sample. The emission and excitation spectra were recorded by a FluoroMax-4 (Jobin-Yvon) spectrofluorometer. Photoluminescence quantum yield (PLQY) measurements were measured using the quanta- φ (HORIBA) integrating sphere accessory, attached to the “FluoroMax-4” Horiba Jobin Yvon spectrofluorometer.

Time-resolved emission (TRES) measurements were measured by exciting **1** with 40 ps-pulsed (<1 mW, 40 MHz repetition rate) diode lasers (PicoQuant, Germany) centered at 371 and 433 nm. The system was equipped with a laser driver (PDL820B, PicoQuant, Germany) for burst operation that allows the measurement of luminescence decays at time windows up to several seconds. The emission decays were collected and analyzed through a TCSPC and multi-channel scaling board (TimeHarp260 (nano), PicoQuant, Berlin, Germany). The fluorescence signal was gated at a magic angle (54.7°) and monitored at 90° with respect to the excitation beam at discrete emission wavelengths. The experimental decays were analyzed using a single or biexponential functions.

The low-temperature steady-state and time-resolved measurements were performed using a variable-temperature liquid nitrogen-cooled cryostat (OptistatDN, Oxford Instruments, England) connected to ITC601 temperature controller (Oxford instruments, England).

EPR Spectroscopy

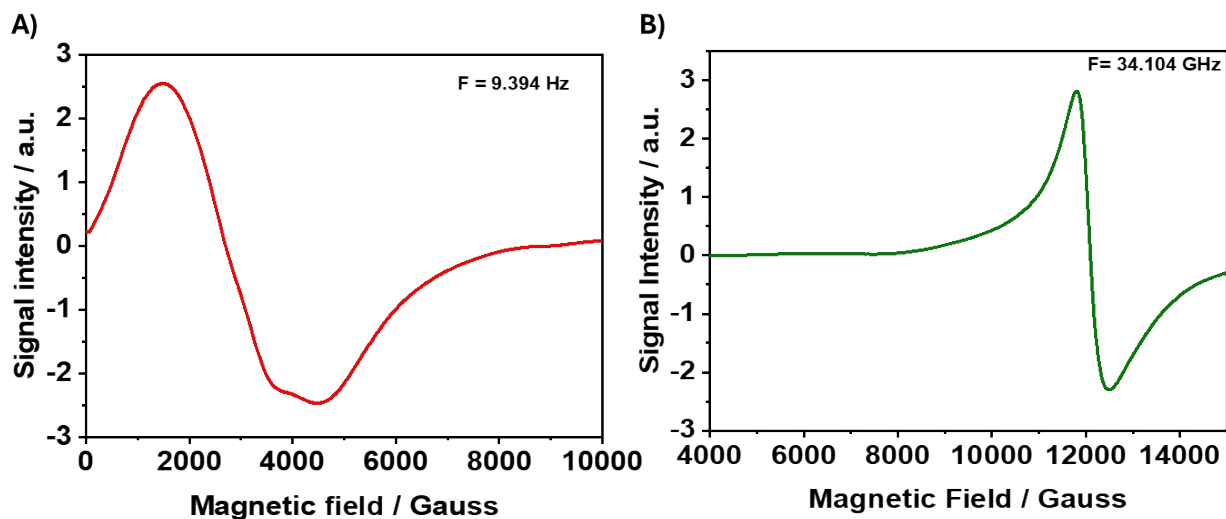


Figure S1. Electron-spin paramagnetic resonance (EPR) at **A)** X-band and **B)** Q-band of **1** at RT.

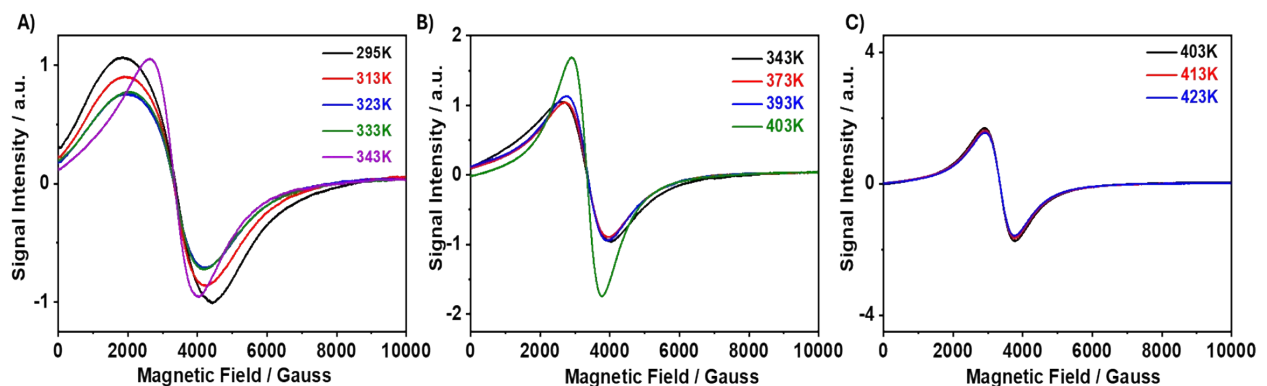


Figure S2. Thermal evolution of the X-band EPR spectra of **1** from 295 to 423 K. Notice the transition between 333 and 343 K.

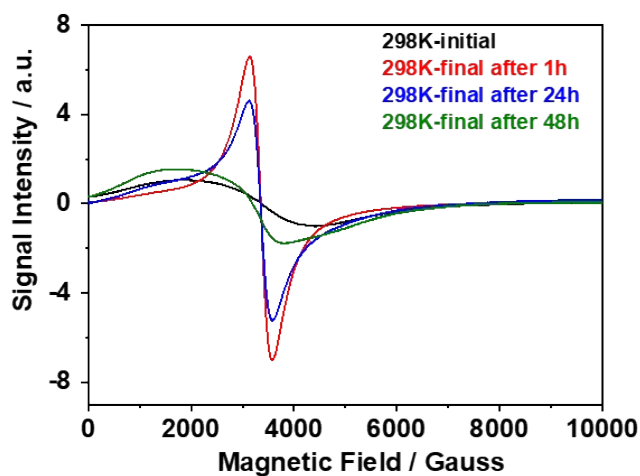


Figure S3. X-band EPR spectra recorded before and after the sample was heated to 423 K and left at room temperature for the time indicated.

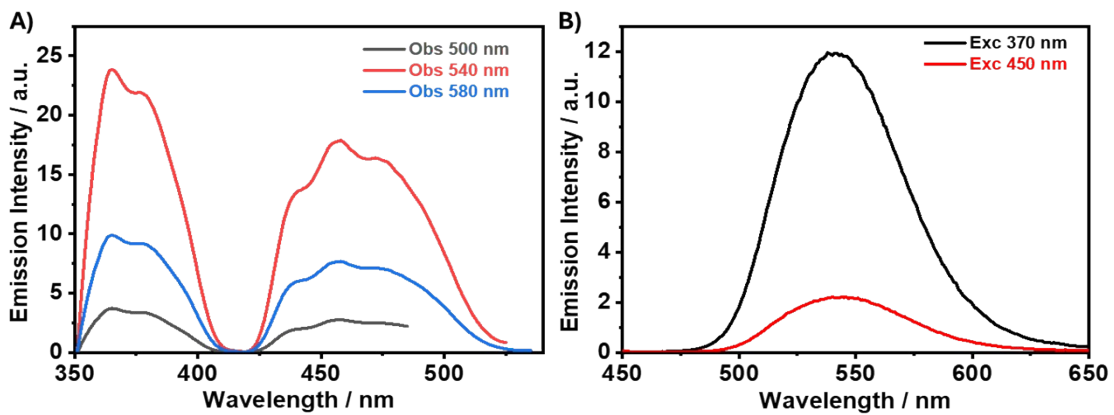


Figure S4. **A)** Excitation spectra of **1** collected at the indicated emission wavelengths. **B)** Emission spectra of **1** upon excitation at the indicated wavelengths.

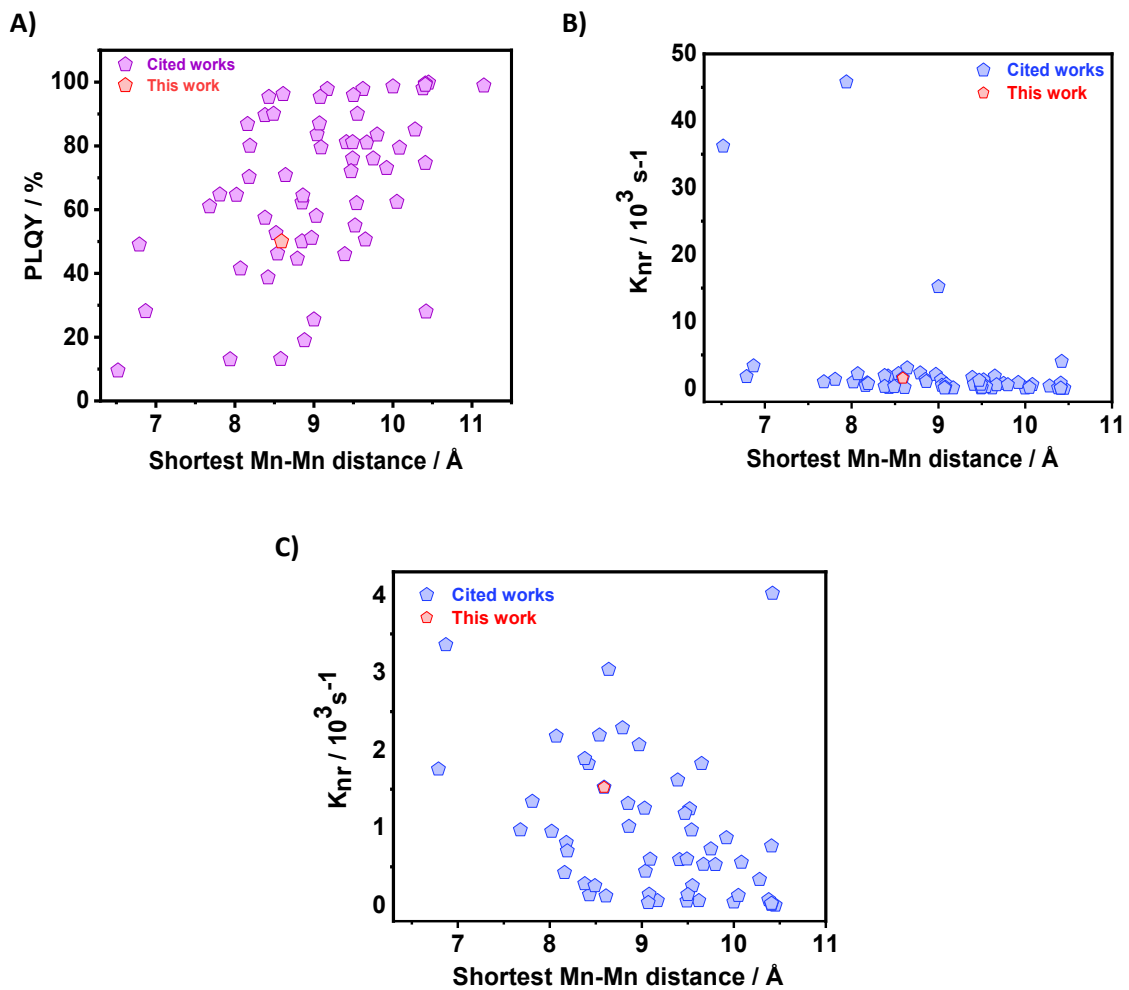


Figure S5. Variation of the PLQY (A) and the non-radiative rate constant, κ_{nr} (B) with the shortest Mn-Mn distance in reported Mn-Based tetrahedral hybrid perovskites. (C) is a zoom of (B) without the data having κ_{nr} larger than $4 \times 10^3 \text{ s}^{-1}$. The data of **1** are in red color.

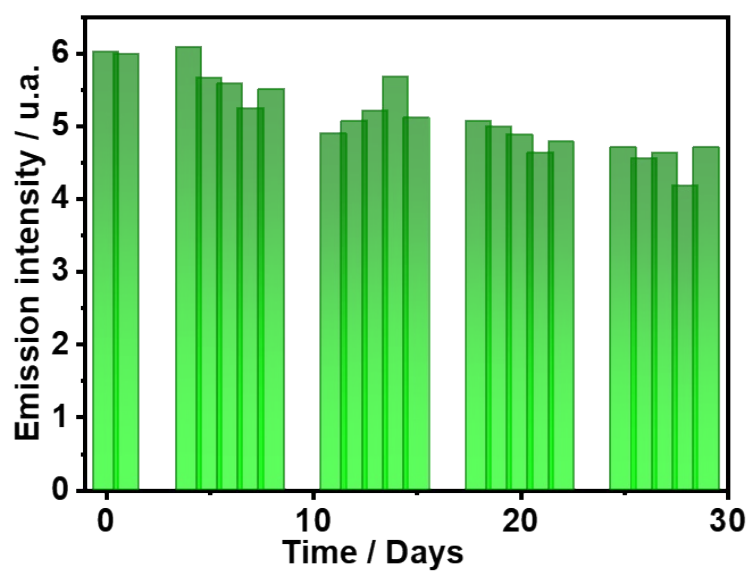


Figure S6. Change in the green emission intensity maximum of **1** with days. The powder was in permanent contact with ambient conditions of humidity, temperature and light.

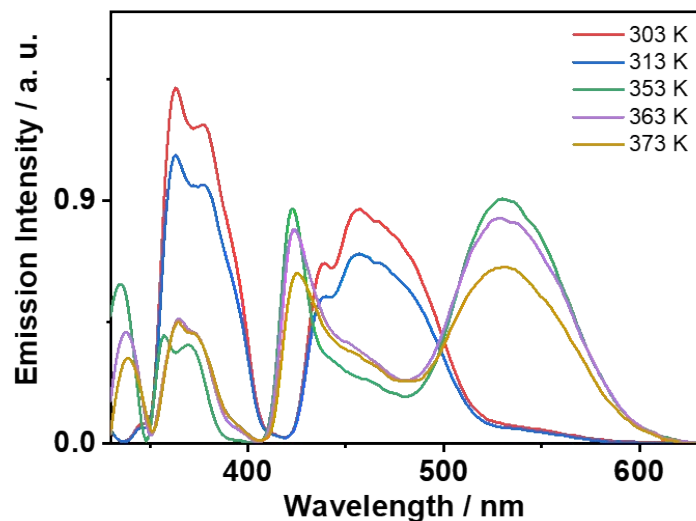


Figure S7. Excitation spectra of **1** gated at 650 nm and at different temperatures as indicated.

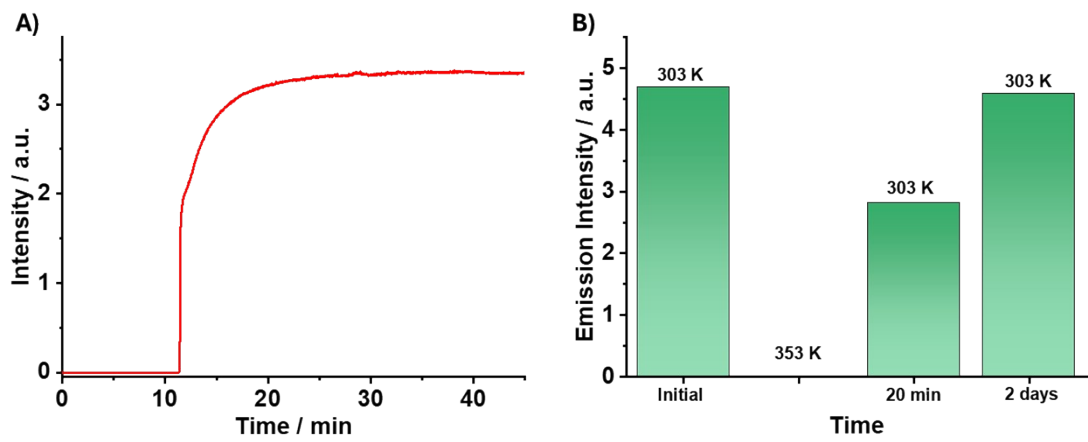


Figure S8. Recovery of the emission intensity maximum (at 540 nm) during the cooling process of **1** in minutes (A) and in days (B).

Table S1. Crystal data and structure refinement for **1** at 296K.

(DPA) ₂ MnBr ₄	
Empirical formula	Br ₄ Mn·2(C ₆ H ₁₆ N)
Formula Mass/ g.mol ⁻¹	<i>M</i> _r =578.97
Crystal system	Monoclinic
Space group	<i>P</i> 2 ₁ / <i>n</i>
<i>a</i> /Å	12.3187 (2)
<i>b</i> /Å	13.9925 (2)
<i>c</i> /Å	14.1168 (2)
β/°	107.7259 (18)
<i>V</i> / Å ³	2317.77 (7)
<i>Z</i>	4
<i>T</i> / K	296
λ / Å	1.54184
<i>F</i> (000)	1132
μ/ mm ⁻¹	12.64
D _x / Mg m ⁻³	1.659
<i>R</i> _{int}	0.040
R[F ² > 2σ(F ²)]	0.038
wR(F ²)	0.103
independent reflections	4239
Δρ _{max} , Δρ _{min} / e Å ⁻³	1.82, -1.46

$$w = 1/[\sigma^2(F_o^2) + (0.0604P)^2 + 2.7792P] \text{ where } P = (F_o^2 + 2F_c^2)/3$$

Table S2. Fractional atomic coordinates and isotropic or equivalent isotropic displacement parameters (Å²) for **1**.

	<i>x</i>	<i>y</i>	<i>z</i>	<i>U</i> _{iso} */* <i>U</i> _{eq}
Br1	-0.00736 (6)	0.30104 (5)	0.59498 (4)	0.1048 (2)
Br2	0.02787 (5)	0.11033 (4)	0.81399 (5)	0.0983 (2)
Br3	0.27026 (4)	0.31964 (3)	0.83252 (4)	0.08011 (16)
Br4	-0.02819 (7)	0.38892 (6)	0.87222 (6)	0.1316 (3)
Mn1	0.06045 (6)	0.28164 (5)	0.77891 (5)	0.0722 (2)
C1	0.0767 (7)	0.6468 (5)	0.8049 (6)	0.141 (3)
H1A	0.060899	0.702202	0.762829	0.211*
H1B	0.101953	0.666503	0.873314	0.211*
H1C	0.008826	0.609034	0.792933	0.211*
C2	0.1696 (5)	0.5876 (4)	0.7823 (4)	0.1059 (17)
H2A	0.239656	0.624307	0.798487	0.127*
H2B	0.183732	0.530476	0.823162	0.127*
C3	0.1352 (4)	0.5602 (4)	0.6755 (4)	0.0918 (14)

H3A	0.124805	0.617516	0.635155	0.110*
H3B	0.062688	0.526928	0.658796	0.110*
C4	0.1965 (5)	0.4730 (4)	0.5444 (4)	0.0935 (14)
H4A	0.199488	0.530770	0.507309	0.112*
H4B	0.119917	0.447320	0.519722	0.112*
C5	0.2784 (6)	0.4022 (5)	0.5271 (5)	0.121 (2)
H5A	0.276850	0.344956	0.565545	0.146*
H5B	0.354772	0.428468	0.550194	0.146*
C6	0.2504 (8)	0.3756 (7)	0.4177 (6)	0.167 (3)
H6A	0.252703	0.431975	0.379531	0.250*
H6B	0.175655	0.347966	0.395075	0.250*
H6C	0.305367	0.330282	0.409523	0.250*
N1	0.2216 (3)	0.4972 (3)	0.6514 (3)	0.0839 (10)
H1D	0.289080	0.526151	0.671764	0.101*
H1E	0.227137	0.443159	0.685708	0.101*
C7	0.1182 (9)	1.1165 (6)	0.4293 (8)	0.184 (4)
H7A	0.095210	1.127404	0.358830	0.276*
H7B	0.189750	1.147668	0.459801	0.276*
H7C	0.061534	1.141778	0.456399	0.276*
C8	0.1306 (7)	1.0132 (5)	0.4490 (5)	0.135 (2)
H8A	0.057353	0.982675	0.419818	0.162*
H8B	0.152577	1.002884	0.520275	0.162*
C9	0.2165 (5)	0.9670 (4)	0.4089 (5)	0.1052 (17)
H9A	0.195471	0.979270	0.337962	0.126*
H9B	0.289901	0.996847	0.439360	0.126*
C10	0.2986 (5)	0.8098 (5)	0.3760 (5)	0.1106 (19)
H10A	0.372178	0.840908	0.390329	0.133*
H10B	0.262454	0.813127	0.304666	0.133*
C11	0.3176 (7)	0.7086 (5)	0.4044 (6)	0.137 (2)
H11A	0.353094	0.705786	0.475825	0.165*
H11B	0.243673	0.678032	0.390183	0.165*
C12	0.3852 (9)	0.6530 (7)	0.3588 (8)	0.190 (4)
H12A	0.346222	0.646965	0.288991	0.284*
H12B	0.397500	0.590701	0.388670	0.284*
H12C	0.457207	0.683994	0.368226	0.284*
N2	0.2287 (4)	0.8639 (3)	0.4250 (3)	0.1047 (14)
H2C	0.159174	0.838542	0.406057	0.126*
H2D	0.257496	0.854120	0.490150	0.126*

Table S3. Atomic displacement parameters (\AA^2) for **1**.

	U^{11}	U^{22}	U^{33}	U^{12}	U^{13}	U^{23}
Br1	0.1161 (4)	0.1165 (5)	0.0691 (3)	-0.0199 (3)	0.0092 (3)	0.0115 (3)
Br2	0.0899 (4)	0.0833 (3)	0.1190 (4)	-0.0141 (3)	0.0277 (3)	0.0124 (3)
Br3	0.0655 (3)	0.0777 (3)	0.0882 (3)	0.0012 (2)	0.0100 (2)	0.0027 (2)
Br4	0.1317 (6)	0.1281 (6)	0.1537 (6)	0.0133 (4)	0.0714 (5)	-0.0324 (5)
Mn1	0.0672 (4)	0.0742 (4)	0.0694 (4)	0.0005 (3)	0.0121 (3)	-0.0009 (3)
C1	0.158 (6)	0.112 (5)	0.181 (7)	0.026 (4)	0.093 (6)	0.000 (5)
C2	0.128 (5)	0.084 (3)	0.116 (4)	0.015 (3)	0.054 (4)	0.011 (3)
C3	0.092 (3)	0.069 (3)	0.113 (4)	0.007 (2)	0.027 (3)	0.009 (3)
C4	0.101 (4)	0.094 (3)	0.085 (3)	-0.010 (3)	0.027 (3)	0.006 (3)
C5	0.118 (5)	0.132 (5)	0.123 (5)	-0.003 (4)	0.049 (4)	-0.024 (4)
C6	0.198 (9)	0.181 (8)	0.144 (7)	-0.038 (7)	0.085 (6)	-0.053 (6)
N1	0.083 (2)	0.081 (2)	0.089 (3)	0.0052 (19)	0.029 (2)	0.0135 (19)
C7	0.228 (11)	0.126 (7)	0.205 (10)	0.051 (7)	0.077 (8)	0.036 (6)
C8	0.170 (7)	0.125 (5)	0.110 (5)	0.016 (5)	0.043 (5)	-0.010 (4)
C9	0.084 (3)	0.106 (4)	0.120 (4)	-0.006 (3)	0.024 (3)	0.029 (3)
C10	0.086 (3)	0.139 (5)	0.114 (4)	0.015 (3)	0.042 (3)	0.030 (4)
C11	0.160 (7)	0.121 (6)	0.145 (6)	0.003 (5)	0.066 (5)	-0.019 (5)
C12	0.193 (9)	0.173 (8)	0.246 (12)	0.047 (7)	0.130 (9)	0.016 (8)
N2	0.136 (4)	0.096 (3)	0.091 (3)	-0.020 (3)	0.047 (3)	-0.011 (2)

Table S4. Geometric parameters (\AA , $^\circ$) for **1**.

Br1—Mn1	2.4886 (8)	C4—N1	1.485 (6)
Br2—Mn1	2.5046 (9)	C5—C6	1.523 (9)
Br3—Mn1	2.5189 (8)	C7—C8	1.470 (10)
Br4—Mn1	2.4609 (9)	C8—C9	1.491 (9)
C1—C2	1.523 (8)	C9—N2	1.461 (7)
C2—C3	1.487 (8)	C10—C11	1.471 (9)
C3—N1	1.499 (6)	C10—N2	1.468 (7)
C4—C5	1.486 (8)	C11—C12	1.427 (10)
Br1—Mn1—Br2	106.72 (3)	N1—C4—C5	112.2 (5)
Br1—Mn1—Br3	106.15 (3)	C4—C5—C6	112.0 (6)
Br2—Mn1—Br3	110.74 (3)	C4—N1—C3	115.0 (4)
Br4—Mn1—Br1	115.42 (4)	C7—C8—C9	113.6 (7)
Br4—Mn1—Br2	110.74 (4)	N2—C9—C8	114.9 (5)
Br4—Mn1—Br3	107.00 (3)	N2—C10—C11	115.8 (5)
C3—C2—C1	110.7 (6)	C12—C11—C10	117.9 (7)
C2—C3—N1	112.3 (4)	C9—N2—C10	118.9 (5)

C1—C2—C3—N1	-176.9 (5)	C7—C8—C9—N2	-178.5 (7)
C2—C3—N1—C4	-175.7 (4)	C8—C9—N2—C10	171.3 (6)
C5—C4—N1—C3	-173.7 (5)	C11—C10—N2—C9	173.4 (6)
N1—C4—C5—C6	178.5 (5)	N2—C10—C11—C12	-179.9 (8)

Table S5. Hydrogen-bond geometry (\AA , $^\circ$) for **1**.

D—H…A	D—H	H…A	D…A	D—H…A
C2—H2B…Br3	0.97	3.13	3.945 (5)	143
C3—H3A…Br3 ⁱ	0.97	3.09	3.825 (5)	134
C4—H4B…Br1	0.97	2.96	3.701 (5)	134
N1—H1D…Br2 ⁱ	0.89	2.50	3.369 (4)	166
N1—H1E…Br3	0.89	2.63	3.484 (4)	162
C9—H9B…Br4 ⁱⁱ	0.97	3.13	3.901 (5)	138
C11—H11B…Br1 ⁱⁱⁱ	0.97	3.00	3.827 (8)	144
N2—H2C…Br1 ⁱⁱⁱ	0.89	2.70	3.518 (5)	153
N2—H2D…Br3 ⁱ	0.89	2.67	3.475 (5)	151

Symmetry codes: (i) $-x+1/2, y+1/2, -z+3/2$; (ii) $x+1/2, -y+3/2, z-1/2$; (iii) $-x, -y+1, -z+1$.

Table S6. Comparison of the emission properties of **1** with those of reported Mn-Based tetrahedral hybrid perovskites and Mn-Mn distance.

Hybrid perovskites	Mn-Mn distance (\AA)	$\lambda_{\text{Em}}(\text{nm})$	PLQY (%)	Lifetime (ms)	$K_{\text{nr}} (10^3 \text{ s}^{-1})$	Ref.
(3AMP)MnBr ₄	6.52	514	9.5	0.025	36.2	³
Cs ₃ MnBr ₅	6.79	520	49	0.290	1.76	⁴
(EPY) ₂ MnBr ₄	6.87	515	28.1	0.214	3.36	⁵
(3MP) MnBr ₄	7.94	523	13	0.019	45.79	³
(C ₁₃ H ₂₆ N) ₂ MnBr ₄	8.02	515	64.6	0.370	0.96	⁶
(PMMIM) ₂ MnBr ₄	8.18	515	70.2	0.367	0.81	⁵
(HQ) ₂ MnBr ₄	8.42	545	38.7	0.335	1.83	⁷
(IPTMA) ₂ MnBr ₄	8.52	497	52.6	-	-	⁸
(C ₁₃ H ₁₄ N) ₂ MnBr ₄	8.54	539	46.2	0.245	2.20	⁶

Hybrid perovskites	Mn-Mn distance (Å)	$\lambda_{\text{Em}}(\text{nm})$	PLQY (%)	Lifetime (ms)	$K_{\text{nr}} (10^3 \text{ s}^{-1})$	Ref.
$[(\text{CH}_2)_4\text{N}(\text{CH}_2)_4]_2\text{MnBr}_4$	8.58	525	13.1	-	-	⁹
$(\text{TMPEA})_2\text{MnBr}_4$	8.64	520	70.8	0.096	3.04	³
$(\text{MeQ})_2\text{MnBr}_4$	8.79	528	44.6	0.242	2.29	⁷
$(\text{DIPA})_2\text{MnBr}_4$	8.85	525	62.2	$1.4 \cdot 10^{-6}$	--	¹⁰
$(\text{CH}_2\text{CH}_3)_3\text{NH}_2\text{MnBr}_4$	8.85	528	50	0.380	1.32	¹¹
$(\text{EtQ})_2\text{MnBr}_4$	8.86	528	64.4	0.349	1.02	⁷
$\text{C}_8\text{H}_{20}\text{N}_2\text{MnBr}_4$	8.88	520	19	$3.9 \cdot 10^{-6}$	--	¹²
$(\text{BTMA})_2\text{MnBr}_4$	8.97	519	51.1	0.236	2.07	³
$(\text{HEP})_2\text{MnBr}_4$	9.00	519	25.5	0.049	15.20	³
$(\text{C}_9\text{H}_{14}\text{N})_2\text{MnBr}_4$	9.03	521	58	0.335	1.25	⁵
$(\text{FETQ})_2\text{MnBr}_4$	9.04	516	83.6	0.370	0.44	⁷
$(\text{EMMIM})_2\text{MnBr}_4$	9.09	511	79.5	0.343	0.60	⁵
$(\text{BTEA})_2\text{MnBr}_4$	9.39	515	46	0.334	1.62	¹³
$(\text{C}_9\text{NH}_{20})_2\text{MnBr}_4$	9.41	528	81.1	0.319	0.59	¹⁴
$(\text{TPA})_2\text{MnBr}_4$	9.54	520	62	0.390	0.97	¹⁵
$(\text{DPA})_2\text{MnBr}_4$	8.59	537	50	0.328	1.52	This work
$(\text{BTEA})_2\text{MnBr}_4$	9.62	521	97.8	0.346	0.06	¹⁶
$(\text{BMPR})_2\text{MnBr}_4$	9.65	527	50.6	0.270	1.83	¹³
$(\text{C}_{12}\text{H}_{28}\text{N})_2\text{MnBr}_4$	9.75	511	76	0.329	0.73	⁵
$(\text{HTPP})_2\text{MnBr}_4$	>10	521	98.6	0.307	0.05	¹⁷
$(\text{C}_8\text{H}_{20}\text{N})_2\text{MnBr}_4$	10.28	515	85.1	0.443	0.34	¹⁸
$(\text{C}_{24}\text{H}_{20}\text{P})_2\text{MnBr}_4$	10.45	515	99.8	0.372	0.01	¹⁹
$(\text{PP})_3\text{MnBr}_5$	9.92	510	73	0.309	0.87	²⁰
$(\text{CP})_2\text{MnBr}_4$	10.42	525	28	0.179	4.02	²⁰

Hybrid perovskites	Mn-Mn distance (Å)	$\lambda_{\text{Em}}(\text{nm})$	PLQY (%)	Lifetime (ms)	$K_{\text{nr}} (10^3 \text{ s}^{-1})$	Ref.
$(\text{C}_5\text{H}_{14}\text{N}_3)_2\text{MnBr}_4$	8.16	528	86.8	0.310	0.42	²¹
$[\text{P14}] [\text{MnBr}_4]$	9.67	520	81	0.358	0.53	²²
$[\text{PP14}] [\text{MnBr}_4]$	9.52	527	55	0.361	1.25	²²
$(\text{TPP})_2\text{MnBr}_4$	10.38	520	98	0.265	0.08	²³
$(\text{DMAEMP})\text{MnCl}_4$	9.49	525	81.1	3.260	0.06	²⁴
$(\text{TMG})_2\text{MnBr}_4$	9.55	526	90.0	0.390	0.26	²⁵
$(\text{MTP})_2\text{MnBr}_4$	10.41	516	99.5	0.331	0.02	²⁶
$(\text{BTEA})_2\text{MnBr}_4$	9.17	521	97.8	0.346	0.06	²⁷
$\text{o-C}_{44}\text{H}_{38}\text{P}_2\text{MnBr}_4$	9.50	517	95.9	0.290	0.14	²⁸
$(\text{MTP})_2\text{MnCl}_4$	10.41	512	74.6	0.331	0.77	²⁹
$(\text{pe-ted})_2\text{MnBr}_4$	9.08	529	95.3	0.324	0.15	³⁰
$[\text{Pr}(\text{MIm})_2]\text{MnBr}_4$	8.43	521	95.3	0.338	0.14	³¹
$[\text{Pr}(\text{EIm})_2]_2\text{MnBr}_4$	8.19	522	80.0	0.284	0.70	³¹
$[\text{Bu}(\text{MIm})_2]\text{MnBr}_4$	8.61	532	96.2	0.308	0.12	³¹
$(\text{C}_6\text{H}_8\text{N})_2\text{MnBr}_4$	7.81	525	64.7	0.263	1.34	³²
$[4\text{-MTPP}]_2\text{MnBr}_4$	10.083	522	79.4	0.369	0.56	³³
$(\text{DMML})_2\text{MnBr}_4$	8.07	522	41.5	0.268	2.18	³⁴
$[\text{CH}_3\text{Ph}_3\text{P}]_2\text{MnBr}_4$	9.80	517	83.5	0.312	0.53	³⁵
$(\text{C}_8\text{H}_{20}\text{N})_2\text{MnCl}_4$	9.07	520	87	3.42	0.04	³⁶
$\text{C}_{16}\text{H}_{38}\text{N}_2\text{MnBr}_4$	9.49	534	76	0.4	0.6	³⁷
$\text{C}_{12}\text{H}_{30}\text{N}_2\text{MnBr}_4$	7.68	530	61	0.400	0.98	³⁷
$(2\text{-DMAP})_2\text{MnBr}_4$	8.38	525	57.4	0.225	1.90	³⁸
$[\text{BTMA}]_2\text{MnBr}_4$	9.47	519	72	0.236	1.19	²⁷
$(\text{C}_{21}\text{H}_{22}\text{P})_2\text{MnBr}_4$	11.15	511	98.9	0.380	0.029	³⁹
$(\text{C}_2\text{H}_{22}\text{P})_2\text{MnBr}_4$	10.41	512	99.1	0.329	0.027	⁴⁰

Hybrid perovskites	Mn-Mn distance (Å)	λ_{Em} (nm)	PLQY (%)	Lifetime (ms)	$K_{nr} (10^3 \text{ s}^{-1})$	Ref.
$(\text{C}_{25}\text{H}_{22}\text{P})_2\text{MnCl}_4$	10.05	512	62.4	2.887	0.13	⁴¹
TA_2MnBr_4	8.38	525	89.61	0.370	0.28	⁴²
$(\text{TMG})_2\text{MnBr}_4$	8.49	527	90.02	0.390	0.26	⁴²

References

- O. Dolomanov, L. Bourhis, R. Gildea, J. Howard and H. Puschmann, *J. Appl. Cryst. J. Appl. Cryst.*, 2009, **42**, 339-341.
- G. M. Sheldrick, *Acta Crystallogr C Struct Chem*, 2015, **71**, 3-8.
- L. Mao, P. Guo, S. Wang, A. K. Cheetham and R. Seshadri, *J. Am. Chem. Soc.*, 2020, **142**, 13582-13589.
- B. Su, M. S. Molokeev and Z. Xia, *J. Mater. Chem. C*, 2019, **7**, 11220-11226.
- Y.-Y. Ma, Y.-R. Song, W.-J. Xu, Q.-Q. Zhong, H.-Q. Fu, X.-L. Liu, C.-Y. Yue and X.-W. Lei, *J. Mater. Chem. C*, 2021, **9**, 9952-9961.
- Q. Ren, J. Zhang, Y. Mao, M. S. Molokeev, G. Zhou and X. M. Zhang, *Nanomaterials*, 2022, **12** (18), 3142.
- J.-Y. Li, C.-F. Wang, H. Wu, L. Liu, Q.-L. Xu, S.-Y. Ye, L. Tong, X. Chen, Q. Gao, Y.-L. Hou, F.-M. Wang, J. Tang, L.-Z. Chen and Y. Zhang, *Adv. Funct. Mater.*, 2021, **31**, 2102848.
- Y.-Y. Luo, Z.-X. Zhang, C.-Y. Su, W.-Y. Zhang, P.-P. Shi, Q. Ye and D.-W. Fu, *J. Mater. Chem. C*, 2020, **8**, 7089-7095.
- L. Xu, J.-X. Gao, X.-G. Chen, X.-N. Hua and W.-Q. Liao, *Dalton Trans.*, 2018, **47**, 16995-17003.
- C. Jiang, N. Zhong, C. Luo, H. Lin, Y. Zhang, H. Peng and C.-G. Duan, *ChemComm.*, 2017, **53**, 5954-5957.
- M.-H. Jung, *Dalton Trans.*, 2023, **52**, 3855-3868.
- H. Peng, B. Zou, Y. Guo, Y. Xiao, R. Zhi, X. Fan, M. Zou and J. Wang, *J. Mater. Chem. C*, 2020, **8**, 6488-6495.
- W. Mao, J. Wang, X. Hu, B. Zhou, G. Zheng, S. Mo, S. Li, F. Long and Z. Zou, *J. Saudi Chem. Soc.*, 2020, **24**, 52-60.
- M. Li, J. Zhou, M. S. Molokeev, X. Jiang, Z. Lin, J. Zhao and Z. Xia, *Inorg. Chem.*, 2019, **58**, 13464-13470.
- A. B. Abdelhadi, M. Gutiérrez, B. Cohen, L. Lezama, M. Lachkar and A. Douhal, *Journal of Materials Chemistry C*, 2024, **12**, 286-295.
- Y. Guo, J. Wu, W. Liu and S.-P. Guo, *Inorg. Chem.*, 2022, **61**, 11514-11518.
- J.-B. Luo, J.-H. Wei, Z.-Z. Zhang, Z.-L. He and D.-B. Kuang, *ngew. Chem.*, 2023, **62**, e202216504.
- T. Jiang, W. Ma, H. Zhang, Y. Tian, G. Lin, W. Xiao, X. Yu, J. Qiu, X. Xu, Y. Yang and D. Ju, *Adv. Funct. Mater.*, 2021, **31**, 2009973.
- G. Zhou, Z. Liu, M. S. Molokeev, Z. Xiao, Z. Xia and X.-M. Zhang, *J. Mater. Chem. C*, 2021, **9**, 2047-2053.
- W. Liu, H. Xie, W. Cai, R. Zhang, B. Xu and C. Yang, *Journal of Alloys and Compounds*, 2023, **968**, 172173.
- G. Zhou, J. Ding, X. Jiang, J. Zhang, M. S. Molokeev, Q. Ren, J. Zhou, S. Li and X.-M. Zhang, *Journal of Materials Chemistry C*, 2022, **10**, 2095-2102.

22. L.-K. Gong, Q.-Q. Hu, F.-Q. Huang, Z.-Z. Zhang, N.-N. Shen, B. Hu, Y. Song, Z.-P. Wang, K.-Z. Du and X.-Y. Huang, *Chemical Communications*, 2019, **55**, 7303-7306.
23. K. Han, K. Sakhatskyi, J. Jin, Q. Zhang, M. V. Kovalenko and Z. Xia, *Advanced Materials*, 2022, **34**, 2110420.
24. H.-M. Pan, Q.-L. Yang, X.-X. Xing, J.-P. Li, F.-L. Meng, X. Zhang, P.-C. Xiao, C.-Y. Yue and X.-W. Lei, *Chemical Communications*, 2021, **57**, 6907-6910.
25. X. Cheng, X. Chang, Y. Lin, L. Lv, L. Cong, Y. Jia, J. Yin, J. Li and B. B. Cui, *Small*, 2024, **20**, 2307216.
26. W. Zhang, P. Sui, W. Zheng, L. Li, S. Wang, P. Huang, W. Zhang, Q. Zhang, Y. Yu and X. Chen, *Angewandte Chemie International Edition*, 2023, **62**, e202309230.
27. Y. Guo, J. Wu, W. Liu and S.-P. Guo, *Inorganic Chemistry*, 2022, **61**, 11514-11518.
28. P. Fu, Y. Sun, Z. Xia and Z. Xiao, *The Journal of Physical Chemistry Letters*, 2021, **12**, 7394-7399.
29. A. A. Karluk, S. Thomas, A. Shkurenko, B. E. Hasanov, J. Mahmood, M. Eddaoudi and C. T. Yavuz, *Journal of Materials Chemistry C*, 2025, **13**, 2165-2171.
30. J. Fan, H. Tong, Z. Zhou, Y. Lv, H. Li, W. Liu and G. Ouyang, *Small*, 2025, **21**, 2407565.
31. Z. Huang, Y. Wang, P. Du, W. Gao, P. Niu, D. Xu, L. Wang, Y. Deng and A. Song, *Inorganic Chemistry*, 2024, **63**, 21059-21069.
32. Y. Sun, Q. Ma, D. Zhao, P. Gao, Q. Wang, Z. Guo and X. Jiang, *Inorganic Chemistry Frontiers*, 2025, **12**, 291-300.
33. K. Li, Z. Y. Li, H. R. Dong, Y. Chen, Z. G. Li, Y. Q. Chen, R. Feng and W. Li, *Chinese Journal of Chemistry*, 2025, **43**, 501-507.
34. M. M. Lun, H. F. Ni, Z. X. Zhang, J. Y. Li, Q. Q. Jia, Y. Zhang, Y. Zhang and D. W. Fu, *Angewandte Chemie*, 2024, **136**, e202313590.
35. Z. Z. Zhang, Z. L. He, J. B. Luo, J. H. Wei, X. X. Guo, J. H. Chen and D. B. Kuang, *Advanced Optical Materials*, 2024, **12**, 2302434.
36. T. Chang, Y. Dai, Q. Wei, X. Xu, S. Cao, B. Zou, Q. Zhang and R. Zeng, *ACS Applied Materials & Interfaces*, 2023, **15**, 5487-5494.
37. S. Zhang, Y. Zhao, J. Zhou, H. Ming, C.-H. Wang, X. Jing, S. Ye and Q. Zhang, *Chemical Engineering Journal*, 2021, **421**, 129886.
38. Z. L. He, J. H. Wei, Z. Z. Zhang, J. B. Luo and D. B. Kuang, *Advanced Optical Materials*, 2023, **11**, 2300449.
39. M. Wu, J. a. Lai, Y. Pu, Z. Wang, F. Kuang, Y. Zhou, K. An, S. Cao, B. Sun and Z. Liu, *Journal of Materials Chemistry C*, 2025 ,**13**, 11764-11775.
40. J. Fan, H. Li, W. Liu and G. Ouyang, *Angewandte Chemie*, 2025, **137**, e202425661.
41. M. Zhou, H. Jiang, T. Hou, S. Hou, J. Li, X. Chen, C. Di, J. Xiao, H. Li and D. Ju, *Chemical Engineering Journal*, 2024, **490**, 151823.
42. L. Cong, L. Lv, Y. Liu, Y. Jia, X. Chang, Y. Lin, J. Li and B.-B. Cui, *Chemical Engineering Journal*, 2025, **505**, 159672.

Acknowledgment

This work was supported by the following grants: grant PID2020-116519RB-I00 and TED2021-131650B-I00 funded by MICIU/AEI/10.13039/501100011033 and the European Union (EU); grants, SBPLY/23/180225/000196 and SBPLY/21/180501/000108 funded by JCCM and the EU through “Fondo Europeo de Desarrollo Regional” (FEDER); grant 2022-GRIN-34325 funded by UCLM (FEDER). A.B.A. thanks the grant from the Spanish Service for the Internationalization of Education (SEPIE), through the EU Erasmus+ key action program (2020-

1-ES01-KA107-079868), and F.S. thanks Ministerio de Universidades for the FPU21/04332 national fellowship. The authors thank Mr. Miguel Gascón Madrid for his technical assistance in the synthesis of the product and steady-state absorption and emission spectra.

Conflicts of interest

The authors declare no conflict of interest.